The 8th European Congress on Computational Methods in Applied Sciences and Engineering
ECCOMAS Congress 2022
5 – 9 June 2022, Oslo, Norway

EFFECT OF GRAPHITE-PARTICLE MORPHOLOGY ON THERMOMECHANICAL PERFORMANCE OF COMPACTED GRAPHITE IRON: NUMERICAL MODELLING

EVANGELIA NEKTARIA PALKANOGLOU, MINGHUA CAO, KONSTANTINOS P. BAXEVANAKIS AND VADIM V. SILBERSCHMIDT

Wolfson School of Mechanical, Electrical and Manufacturing Engineering
Loughborough University, LE11 3TU, UK
e-mail: v.silberschmidt@lboro.ac.uk, https://www.lboro.ac.uk/departments/meme/staff/vadim-silberschmidt/

Key words: Thermomechanical performance, Compacted graphite iron, Finite element method, Cohesive zone, Inclusion morphology.

Abstract. Compacted graphite iron (CGI) is used in numerous applications, e.g., in the automotive industry, in tools and pipes, thanks to its excellent thermomechanical properties. Despite its extensive industrial use, its fracture at the microscale was not thoroughly investigated. Interfacial debonding is the main mechanism of fracture of CGI at the microscale and is based on the deformational incompatibility between graphite and the surrounding matrix. To study this decohesion, a two-dimensional micromechanical model of elliptical inclusions embedded in a metallic matrix is generated. An elastoplastic response is assumed for both constituents, and cohesive finite elements are applied to the graphite-matrix interface to simulate decohesion. A parametric analysis of interfacial features such as thickness and stiffness is performed to identify the effect of these parameters on debonding. The obtained results provide insights into the thermomechanical behaviour of CGI at the microscale and enable more effective modelling of this engineering alloy.

1 INTRODUCTION

CGI is an alloy widely used in industrial applications mainly thanks to its good thermomechanical properties, excellent wear resistance, and competitive price [1]. CGI is a ferrous alloy containing elements of iron, silicon and carbon, the last in the form of either carbide or graphite. Its microstructure consists of graphite inclusions of different shapes and sizes embedded in a metallic matrix. Three different types of particles are identified based on their morphology: *nodular*, *vermicular*, and *flake* graphite (Figure 1).

Generally, graphite is very soft and brittle. Its limited deformation capacity triggers a mismatch between the inclusions and the surrounding matrix material, leading to debonding at low stress levels. More specifically, thermal debonding can occur even under purely thermal load as a result of a mismatch in the coefficients of thermal expansion (CTE) between the graphite inclusions and the matrix. As decohesion evolves, microcracks appear in the microstructure [2], which then connect, forming larger cracks propagating across the microstructure and potentially resulting in total failure [3].

Interfacial debonding was experimentally confirmed as the main mechanism of fracture in CGI under tensile load [4,5] or fatigue [6,7]. Indeed, decohesion was observed before yielding of the surrounding matrix, between 150 and 200 MPa, under uniaxial tensile conditions [3], and at lower stress levels (50 MPa) under thermomechanical load. In this case, thermal exposure triggered the softening of the microstructure resulting in earlier debonding [2]. Similar observations were reported for ductile cast iron under cyclic loading, where graphite nodules lost their contact with the surface either partially or completely [8].

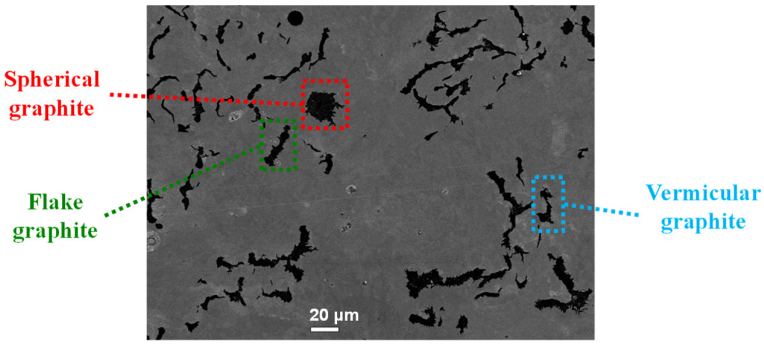

Figure 1: Microstructure of compacted graphite iron (CGI)

Modelling schemes for simulation of the thermomechanical performance of cast irons are classified into *phenomenological* and *micromechanical*, with the main focus being either grey or ductile cast iron. Initial modelling attempts were based only on phenomenological descriptions and involved modification of a yield surface and hardening parameters to consider the effect of microstructural features [9]. However, gradual improvement of experimental techniques for microstructure characterisation encouraged the development of micromechanical modelling schemes, which related the response of each microstructural constituent to experimental observations [10,11]. Most recent micromechanical models focus on fatigue performance and crack-path prediction; however, they do not consider any form of interfacial debonding, especially under thermal loading.

The response of CGI at elevated temperatures significantly deteriorates due to the mismatch of CTEs of its constituents. This mismatch causes interfacial debonding and triggers initiation and propagation of cracks across the microstructure, leading to failure. Despite the fact that most CGI applications are subjected to such loading conditions, graphite decohesion was not considered in existing modelling schemes due to complexity of parameter identification. This lack of knowledge is partially attributed to CGI's complex microstructure, which is difficult to characterise and model adequately. In this paper, thermal debonding is investigated numerically, emphasising the sensitivity of this phenomenon to interfacial parameters, such as thickness and stiffness of interface. The parametric analysis is based on a micromechanical approach, with specific inputs obtained from statistical analysis of scanning electron microscopy (SEM) micrographs, mechanical testing at various temperatures, and nano indentation.

2 METHODOLOGY

2.1 Microstructure characterisation

A set of micrographs of CGI microstructures obtained with SEM were analysed with the image-processing software ImageJ. This software determines the microstructural constituents based on their greyscale shades and evaluates geometrical features of microstructures such as the volume fraction, area, and nodularity of graphite inclusions. Nodularity is a dimensionless parameter related to roundness of particles, ranging from zero to one, defined as the ratio between areas of nodular graphite particles and total graphite area. As the roundness becomes larger, the particle shape becomes more circular, whereas as it decreases, the shape of the inclusion becomes more elliptical. The average values of roundness for micrographs examined in this study are presented in Table 1. The minimum and maximum values of the geometrical features of the examined inclusions are given in Table 2. The obtained results were then employed for the development of a statistically equivalent unit cell [12,13].

Table 1: Average roundness of graphite inclusions

Type of graphite	Flake	Vermicular	Spherical
Roundness	0.0-0.019	0.2-0.79	0.8-1

Table 2: Minimum and maximum values of geometrical parameters of graphite particles in CGI [14]

Volume fraction (%)	Major axis (μm)	Minor axis (μm)	Perimeter (μm)	Area (μm^2)
7-11	0.60-67.96	0.52-28.51	3.54-315.88	0.99-6086.96

2.2 Nano indentation

To identify the interfacial stiffness, nano indentation was performed on specimens made of EN-GJV-450. Its chemical composition and macroscopic properties are listed in Tables 3 and 4, respectively. A short cylindrical sample of diameter 20 mm and length of 10 mm was machined and then grounded with two different grit sizes, P500 (30.2 μm grit size) and P1200 (15.3 μm). Accordingly, the sample was polished with polishing cloths with abrasives of different sizes, ranging from 9 μm to less than 1 μm.

Table 3: Chemical composition (%) of EN-GJV-450 [15]

Fe	C	Si	Cu	Mn	Sn	Cr	Ni	S
92	3.8	2.42	0.917	0.297	0.083	0.025	0.023	0.013
P	Ce	Mg	Al	Ti	V	Mo	Nb	
0.01	0.01	0.009	0.008	0.009	0.008	0.001	0.002	

Table 4: Macroscopic properties of EN-GJV-450 [15]

Property	23 °C	100 °C	400 °C
Ultimate tensile strength (MPa)	450-525	425-500	350-425

0.2% proof stress (MPa)	315-365	290-340	265-315
Elongation (%)	1-2.5	1-2	0.5-1.5
Elastic modulus (GPa)	144-155	140-150	135-145
Thermal conductivity (W/mK)	38	37	36
CTE (10^{-6} per °C)	11	11	12.5

The nano indentation test was performed in a selected area of the microstructure, containing graphite particles and the matrix (Figure 2). The test provided evidence about the presence of an interface between graphite and matrix. The literature lacks information on interface properties since assessment of the response of graphite or matrix was considered more important. Variation of the Young's modulus across the microstructure was identified, with graphitic areas showing the lowest values and matrix regions the highest ones. Additionally, it was observed that the Young's modulus changed gradually from graphitic to matrix areas and vice versa, indicating the existence of an outer layer around graphite, acting as an interface. The values of the Young's modulus at the interface lay between those of graphite and matrix. Therefore, a mean value of 109.4 GPa was calculated with a standard deviation of 36.7 GPa for the Young's modulus of the interface. Despite confirming the existence of an interface, its composition and structure cannot be identified with this type of experiment.

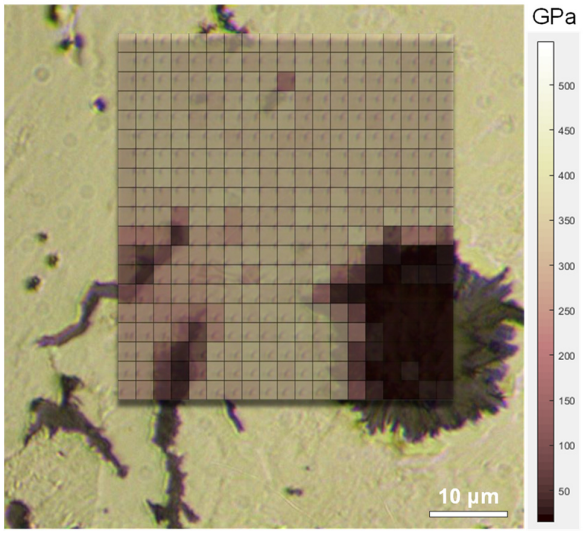

Figure 2: Variation of Young's modulus across the microstructure

2.3 Micromechanical model

Normally, a representative volume element (RVE) encloses a significant number of inclusions [16]. However, due to CGI's complex microstructure, it would be hard to investigate graphite decohesion considering the interaction between graphite inclusions. Such interactions influence the temperature of debonding initiation and affect the impact of other parameters on the evolution of decohesion. Thus, a two-dimensional RVE comprising a single vermicular inclusion embedded in a square domain representing the matrix material was generated for this

work. Although graphite particles of different morphology were identified in the microstructure, vermicular ones were the most common. Therefore, it is rational to assume that a vermicular particle could be representative of a general graphite inclusion based on the results obtained from microstructure characterisation. The geometry of the generated RVE is shown in Figure 3. The dimensions were identified, assuming a volume fraction of 9% based on the results of microstructural characterisation.

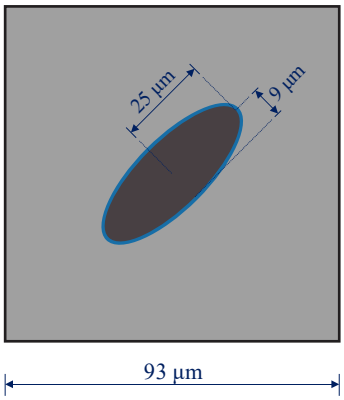

Figure 3: Geometry of developed RVE

Table 5: Constitutive parameters for matrix material and graphite inclusions

Ferrite metallic matrix					
Temperature (°C)	Yield point (MPa)	Yield strain (%)	Young's modulus (GPa)	Poisson's ratio	Coefficient of thermal expansion
50	323.95	0.209			
150	316.84	0.195			
300	301.18	0.225	150	0.25	1.2×10^{-5}
400	265.92	0.178			
500	257.71	0.179			
Graphite					
50	27.56	0.184	15.85	0.2	2.9×10^{-5}

The constitutive behaviour of the metallic matrix was assumed to be elastoplastic, described by the J2 flow theory of plasticity since it can be considered isotropic and ductile. Also, to study thermal debonding effectively, temperature-dependent constitutive data were used for the matrix. Although graphite is soft and brittle, data found in the literature indicated that it can exhibit limited plastic deformation. Thus, elastoplastic behaviour was assumed for graphite particles in this study [10,17]. The constitutive parameters for both graphite and matrix are shown in Table 5. The parameters of the matrix material were obtained from in-house mechanical tests of CGI specimens.

To investigate thermal debonding, a traction-type elastic behaviour was assumed for the interfacial layer [14]. Additionally, to effectively simulate the loss of contact between graphite and matrix domains, a stress-based damage criterion was established resulting in deletion of elements of the interface when its critical value was met. Normally, in a finite-element code,

the damage estimation process is performed by evaluating the magnitude of a damage variable (D) at all Gauss points of an element. This parameter represents the reduction of element's stiffness after material degradation starts and ranges from zero to one. When D becomes nonzero at any of the Gauss points, the element is considered damaged; it is deleted when $D = 1$ at all integration points. The values of the damage criterion applied to the interfacial layer were selected so that the enclosed graphite inclusion remained elastic during the thermal excursion.

Full-integration quadrilateral plane stress elements (CPS4) were used in the unit cell. Cohesive elements following a traction-separation law were employed to simulate the interfacial layer between graphite and matrix domains. After a mesh-convergence study, the model comprised 12218 elements, with 24456 degrees of freedom.

An RVE is considered a representative part of microstructure with a regular pattern and behaviour typical for the entire material. To achieve this, periodic boundary conditions (PBCs) must be implemented along the RVE edges to simulate accurately the surrounding deformation field [16]. PBCs guarantee that the outer edges of the unit cell would remain periodic during deformation. This means that every RVE has the same deformation without overlapping or being separated from its surrounding cells. For an RVE with dimension d, the PBC of any two points x and $x + d$ on its two opposite edges are expressed as [18]

$$\mathbf{u}(x, d) = \mathbf{u}(x) + \bar{\varepsilon} d, \tag{1}$$

$$\mathbf{t}(x, d) = -\mathbf{t}(x), \tag{2}$$

where $\mathbf{u}$ is the displacement and $\mathbf{t}$ is the surface traction. Here, $\bar{\varepsilon}$ denotes the average infinitesimal strain over the volume element and is mostly determined externally.

In this study, a purely thermal load was applied to the RVE to study thermal decohesion and the parameters that affect it. As already discussed, the performance of CGI is primarily affected by elevated temperatures due to its heterogeneous nature. Temperature loading was applied as a field to the entire model, in the form of a linear increase of temperature in the material from 50 °C to 500 °C.

3 RESULTS OF FINITE-ELEMENT SIMULATIONS

3.1 Effect of interfacial stiffness

The effect of interfacial stiffness on graphite debonding is presented in Figure 4. The values used for the stiffness were obtained by nano indentation in CGI specimens and the thickness of the interface for this investigation was 1 μm. Temperature levels at the onset of decohesion (T_d) were normalised using the maximum temperature applied to the unit cell (500 °C). It was found that as the interface became stiffer, the initiation temperature of graphite decohesion decreased. More specifically, for values of interfacial stiffness ranging from some 60 GPa to 100 GPa, an almost linear trend was observed. As the stiffness increased further, the rate of temperature decreased.

This behaviour was attributed to the fact that as the interfacial stiffness increased, the layer became less ductile and had limited deformational capacity. As the temperature increased, the interface could not expand to the same extent as the surrounding matrix. This gradually reduced the contact between the two constituents up to the level of loss of contact between them.

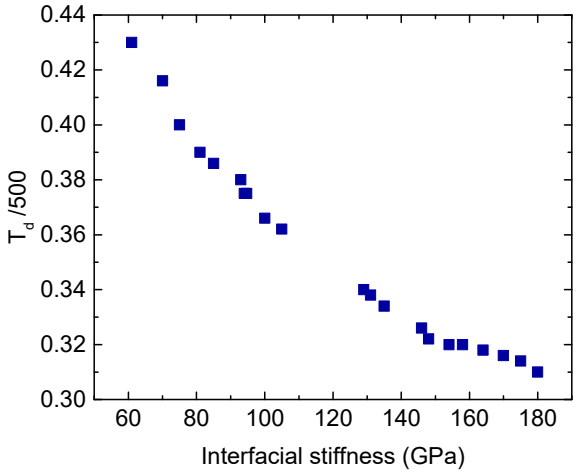

Figure 4: Effect of interfacial stiffness on graphite decohesion (thickness 1 μm)

3.2 Effective of interfacial thickness

The interfacial layer is not clearly observed in micrographs of CGI and its thickness is quite difficult to quantify. Therefore, a parametric analysis was performed to identify its effect on the damage-initiation temperature. The effect of interfacial thickness on the onset of decohesion is presented in Figure 5. The stiffness of the interface in this parametric study was 60 GPa. As the thickness of the interfacial layer increased, the onset of debonding was delayed. For interfacial thickness above 5 μm, no decohesion was observed.

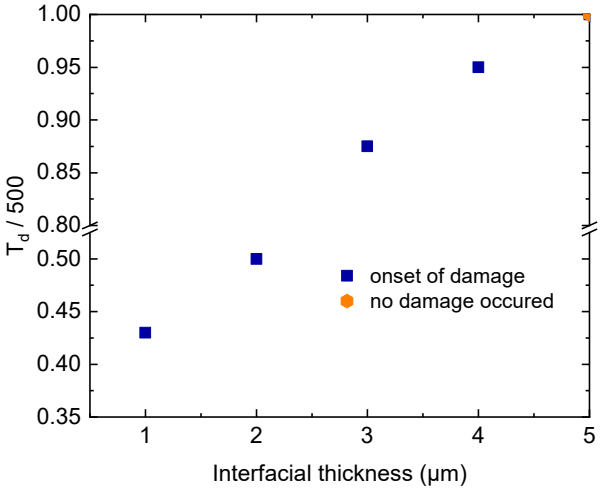

Figure 5: Effect of interfacial thickness on graphite decohesion (stiffness 60 GPa)

Overall, the onset of debonding was significantly affected by the interfacial thickness. This is expected, as a thick interface had a higher load-bearing capacity than a thinner one, which resulted in delaying the occurrence of decohesion.

3.3 Unit cell with stiff interface

Results of numerical analysis of a unit cell with a stiff interface are discussed in this section. The stiffness of the interfacial layer was selected as 180 MPa based on the results of nano indentation, whereas its thickness was 1 μm. The initiation and evolution of decohesion for the RVE with a stiff interface are depicted in Figure 6. The degradation of interfacial strength started at a relatively low temperature (73 °C) compared to an RVE with a less stiff interface [14]. As temperature increased, the strength of interface decreased rapidly, leading to loss of contact in different areas around the inclusion. On the other hand, no plastic deformations were observed in the RVE with stiff interface compared to that with a ductile one, where the plastic strains appeared at 220 °C [14].

A unit cell with a stiff interface had a brittle response to the applied thermal load, with limited deformational capacity, but higher strength. These two competing features justified the earlier onset of graphite decohesion, as well as the absence of any plastic deformations. On the other hand, a less stiff interface could deform to a higher level, leading to a delayed onset of graphite debonding; however, its insufficient strength caused earlier plasticisation.

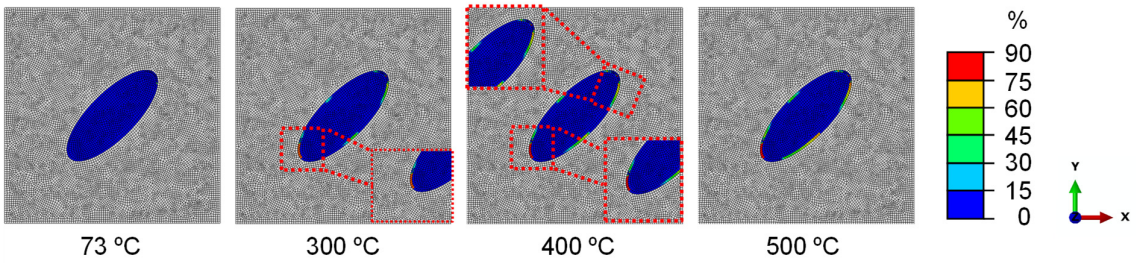

Figure 6: Onset and evolution of graphite debonding for RVE with stiff interface

4 CONCLUSIONS

Thermal debonding between graphite particles and the matrix in CGI, was investigated in this work. A two-dimensional numerical model was generated comprising a vermicular graphite inclusion surrounded by an interfacial layer, embedded in a metallic matrix. The elastoplastic constitutive law was applied to both graphite and matrix domains, whereas the interfacial layer was modelled using cohesive finite elements associated with a damage criterion to account for decohesion.

The onset of debonding between graphite and the matrix occurred at a lower temperature as the stiffness of the interfacial layer increased. Also, as the interfacial layer became thicker, its loading capacity increased so that the initiation of decohesion was delayed or did not appear at all for thickness values above 5 μm.

In conclusion, features of the interface such as its stiffness and thickness affect the graphite decohesion in CGI under thermal exposure.

REFERENCES

[1] McCune, R.C. and Weber, G.A. *Automotive Engine Materials*. Oxford (2001) pp. 426–434.

[2] Qiu, Y., Pang, J.C., Yang, E.N., Li, S.X., and Zhang, Z.F. Transition of tensile strength and damaging mechanisms of compacted graphite iron with temperature. *Mater. Sci. Eng. A* (2016) **677**:290–301.

[3] Qiu, Y., Pang, J.C., Li, S.X., Yang, E.N., Fu, W.Q., Liang, M.X., et al. Influence of thermal exposure on microstructure evolution and tensile fracture behaviors of compacted graphite iron. *Mater. Sci. Eng. A* (2016) **664**:75–85.

[4] Di Cocco, V., Iacoviello, F., Rossi, A., Cavallini, M., and Natali, S. Graphite nodules and fatigue crack propagation micromechanisms in a ferritic ductile cast iron. *Fatigue Fract. Eng. Mater. Struct.* (2013) **36**:893–902.

[5] Zhang, Y., Pang, J.C., Shen, R., Yu, Q., Li, S., and Zhang, Z.Z. Investigation on tensile deformation behavior of compacted graphite iron based on cohesive damage model. *Mater. Sci. Eng. A* (2018) **713**:260–268.

[6] Zou, C.L., Pang, J.C., Zhang, M.X., Qiu, Y., Li, S.X., Chen, L.J., et al. The high cycle fatigue, deformation and fracture of compacted graphite iron: Influence of temperature. *Mater. Sci. Eng. A* (2018) **724**:606–615.

[7] Iacoviello, F. and Di Cocco, V. Influence of the graphite elements morphology on the fatigue crack propagation mechanisms in a ferritic ductile cast iron. *Eng. Fract. Mech.* (2016) **167**:248–258.

[8] Di Cocco, V., Iacoviello, F., Rossi, A., and Iacoviello, D. Macro and microscopical approach to the damaging micromechanisms analysis in a ferritic ductile cast iron. *Theor. Appl. Fract. Mec.* (2014) **69**:26–33.

[9] Frishmuth, R.E. and McLaughlin, P. V Failure analysis of cast irons under general three-dimensional stress states. *J. Eng. Mater. Technol.* (1976) **98**:69–75.

[10] Andriollo, T., Thorborg, J., Tiedje, N.S., and Hattel, J. Modeling of damage in ductile cast iron - The effect of including plasticity in the graphite nodules. *IOP Conf. Ser.: Mater. Sci. Eng.* (2015) **84**:12027.

[11] Andriollo, T., Thorborg, J., and Hattel, J. Modeling the elastic behavior of ductile cast iron including anisotropy in the graphite nodules. *Int. J. Solids Struct.* (2016) **100–101**:523–535.

[12] Kanit, T., Forest, S., Galliet, I., Mounoury, V., and Jeulin, D. Determination of the size of the representative volume element for random composites: statistical and numerical approach. *Int. J. Solids Struct.* (2003) **40**:3647–3679.

[13] Kanouté, P., Boso, D.P., Chaboche, J.L., and Schrefler, B.A. Multiscale methods for composites: a review. *Arch. Comput. Methods Eng.* (2009) **16**:31–75.

[14] Palkanoglou, E.N., Baxevanakis, K.P., and Silberschmidt, V. V Interfacial debonding in compacted graphite iron: effect of thermal loading. *Procedia Struct. Integr.* (2020) **28**:1286–1294.

[15] The British Standards Institution *BS EN 16079: 2011 Founding. Compacted (vermicular) graphite cast irons*. (2011).

[16] Hill, R. Elastic properties of reinforced solids: Some theoretical principles. *J. Mech. Phys.Solids* (1963) **11**:357–372.

[17] Greenstreet, W.L., Yahr, G.T., and Valachovic, R.S. The behavior of graphite under biaxial tension. *Carbon*. (1973) **11**:43–57.
[18] Drago, A. and Pindera, M.-J. Micro-macromechanical analysis of heterogeneous materials: Macroscopically homogeneous vs periodic microstructures. *Compos. Sci. Technol.* (2007) **67**:1243–1263.